

RSC Advances



This is an *Accepted Manuscript*, which has been through the Royal Society of Chemistry peer review process and has been accepted for publication.

Accepted Manuscripts are published online shortly after acceptance, before technical editing, formatting and proof reading. Using this free service, authors can make their results available to the community, in citable form, before we publish the edited article. This *Accepted Manuscript* will be replaced by the edited, formatted and paginated article as soon as this is available.

You can find more information about *Accepted Manuscripts* in the [Information for Authors](#).

Please note that technical editing may introduce minor changes to the text and/or graphics, which may alter content. The journal's standard [Terms & Conditions](#) and the [Ethical guidelines](#) still apply. In no event shall the Royal Society of Chemistry be held responsible for any errors or omissions in this *Accepted Manuscript* or any consequences arising from the use of any information it contains.



Two step label free particle separation in a microfluidic system using elasto-inertial focusing and magnetophoresis†

Received 00th January 20xx,
Accepted 00th January 20xx

DOI: 10.1039/x0xx00000x

www.rsc.org/

Min Jung Kim,^{a,1} Doo Jin Lee,^{a,1} Jae Ryoung Youn,^{*a} and Young Seok Song^{*b}

This study focuses on the separation of different sized particles and cells by employing a facile two step label free separation technique which consists of elasto-inertial particle focusing and magnetophoretic particle repulsion. The elasto-inertial force leads the objects to migrate toward the centerline at the first stage, and the magnetophoretic repulsion force leads them to migrate to the lateral direction depending upon their particle sizes at the second stage in the microchannel. An analytical calculation is carried out to predict the trajectories of different sized particles by considering hydrodynamic viscous drag and magnetophoretic repulsion forces, and compared to the experimental results. Numerical analyses are performed to understand the physics underlying the elasto-inertial particle focusing and the magnetophoretic particle migration.

Introduction

The separation of microparticles suspended in complex fluids is essential in a wide range of chemical and biological applications¹ such as HIV diagnostics,² malaria detection,^{3,4} and cancer diagnostics.⁵ Conventional separation techniques for cells and/or particles employ membrane-based filtering, which has limitations in preventing clogging and pore sizes. In addition, the conventional approaches for the separation rely on labels to identify cells.⁶ Most popular labeling-assisted methods are fluorescence-activated cell sorting (FACS)⁷ and magnetic activated cell sorting (MACS).⁸ However, these methods are time consuming and demand complicated labeling steps, and labels need to be removed from the target cells.⁹ Therefore, such biochemical labeling often causes restriction on practical applications.¹⁰

Recently, new separation techniques based on microfluidic systems have been developed to separate target cells or particles, showing the potential for a point-of-care (POC) diagnostic platform with advantages such as cost effectiveness, high throughput, high purity, and high sensitivity.¹¹⁻¹⁵ Since label free separation techniques take advantage of hydrodynamics of particle-laden fluids, hydrodynamic forces acting on the particles such as inertial, drag, and elastic forces become important as well as particle size, particle density, and

adhesion to a channel wall.¹⁶⁻¹⁸ It is also found that the combination of different types of forces, e.g., inertial/magnetic, inertial/acoustic, inertial/Dean, elastic/inertial forces, could enhance the separation efficiency and purity.^{6, 12, 19-22}

It has been reported that diamagnetic particles suspended in a paramagnetic fluid show negative magnetophoresis under the magnetic field, which causes particle migration towards the direction of weaker magnetic field in the magnetic domain.²³ The magnetophoretic repulsion and hydrodynamic viscous drag forces are more dominant than other forces such as dipole-dipole interactions, gravitational, buoyancy, and diffusion forces.²⁴⁻²⁷ These magnetophoretic repulsion and hydrodynamic viscous drag forces were harnessed for various applications, such as particle trapping, particle separation, and particle focusing.^{9, 28-31}

In recent years, the elasto-inertial focusing of particles mediated by fluid elasticity and inertia has been known to be an efficient technique to focus particles in a microchannel by adding only a small amount of long-chain molecules such as polymers and DNA into Newtonian solutions.³²⁻³⁶ Yang et al.³⁵ firstly named the 'elasto-inertial particle focusing' in their work, where the particle focusing could be characterized by the elasticity number defined as the ratio of the Weissenberg number to the Reynolds number. The elasticity number depends on the rheological properties of the fluid and the characteristic length scale of the channel. Our previous study showed that the combination of the elastic force and Dean drag force yielded a multiplex particle focusing phenomenon induced by the nature of a viscoelastic medium and curved channel geometry.³⁷ Indeed, the particle focusing and separation could be achieved by tuning the rheological properties of the fluids without any external forces and complicated configuration of the devices.

^a Research Institute of Advanced Materials (RIAM), Department of Materials Science and Engineering, Seoul National University, Seoul 08826, Republic of Korea.

^b Department of Fiber System Engineering, Dankook University, Gyeonggi Do 16890, Republic of Korea.

[†]These authors contributed equally to this work.

†Electronic Supplementary Information (ESI) available. See DOI: 10.1039/x0xx00000x

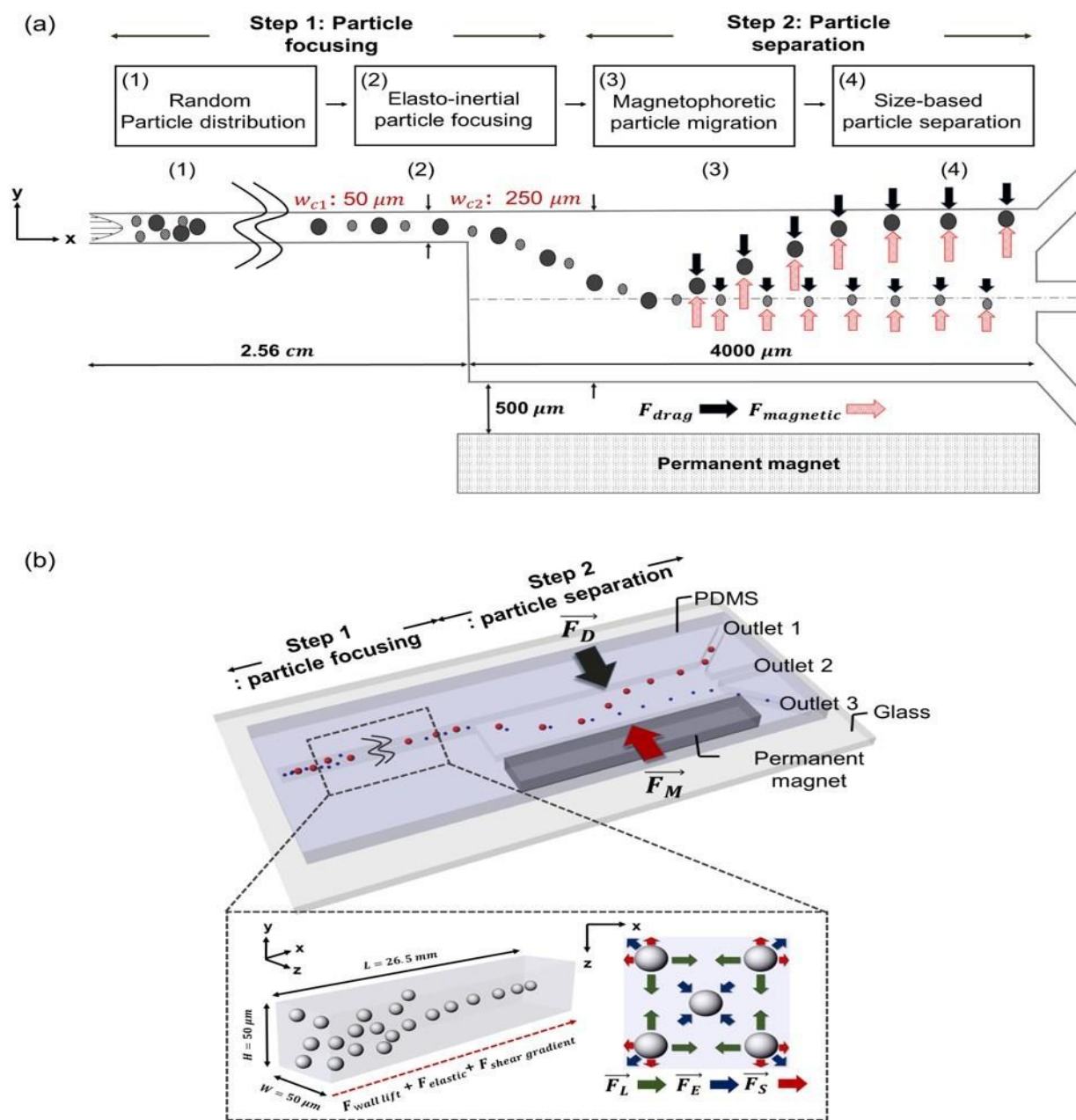


Fig. 1 Channel Design and operating principle for a two-step label free particle separation system. (a) Schematic view of the system: (1) Different size particles in a PEO/ferrofluid medium are introduced into the inlet of a microchannel. (2) When the elasto-inertial force is generated in the narrow channel under $Wi \neq 0$, a single-line particle focusing is observed. (3) Once the magnetic field is applied, particles experience a resulting magnetophoretic repulsion force at the second stage of the channel. Since the magnetic force is dependent on a_p^3 , large particles migrate toward the channel wall. (4) The two different sized particles are collected at different outlets. (b) Schematic illustration of the forces acting on particles: a single line particle focusing is observed at the first stage, in which \vec{F}_L , \vec{F}_E , and \vec{F}_S represent the wall lift, elastic, and shear gradient forces, respectively. \vec{F}_M and \vec{F}_D are dominant factors to determine the position of the particles at the second stage.

In this study, we investigated the focusing and subsequent particle migration behaviours by using the combination of the elastic and magnetorheological properties of fluids to achieve

high separation efficiency of different sized particles. To be more specific, a two-step label free particle separation technique was proposed with the application of two main forces,

the elastic force and the magnetophoretic repulsion force. An analytical calculation and numerical simulation were carried out to reveal the mechanism of two step lateral particle migration in the microfluidic channel.

Results and discussion

Once particles are randomly distributed at the inlet of a microchannel, they are affected by the viscoelastic force and focused at the centerline of the channel. The microfluidic device consists of a straight square channel at the first stage ($h_c = 50 \mu\text{m}$, $w_{c1} = 50 \mu\text{m}$) and an expanded channel at the second stage ($h_c = 50 \mu\text{m}$, $w_{c2} = 250 \mu\text{m}$) (Fig. 1a and 1b). The straight square channel can promote an efficient particle focusing by the elastic force of the fluid since the blockage ratios are 0.1 for $5 \mu\text{m}$ particles and 0.4 for $20 \mu\text{m}$ particles. Once particles are focused at the center, they flow along the streamline to downstream. When the particles encounter the asymmetric expanded channel at the second stage, they are affected by the magnetophoretic repulsion force due to a permanent magnet placed at the bottom of the channel and subsequently move away from the magnet. As the magnetic field is present, the particles experience a resulting magnetophoretic repulsion force ($\vec{F}_M = -V_p \mu_0 (\vec{M}_f \cdot \nabla) \vec{H}$), where V_p is the volume of the

non-magnetic particle, μ_0 is the permeability of free space, \vec{M}_f is the magnetization of magnetic fluid, and \vec{H} is the magnetic field at the center of non-magnetic particles. The magnetophoretic repulsion force acting on the microparticles counteracts the hydrodynamic viscous drag force defined as $\vec{F}_D = 3\pi\eta D_p (\vec{v}_f - \vec{v}_p) f_D$, where η is the viscosity of surrounding fluid, \vec{v}_f is velocity of fluid, \vec{v}_p is the velocity of particles, and f_D is the drag coefficient. The competition between the magnetophoretic repulsion and hydrodynamic viscous drag forces determines the lateral movement of the particles, yielding different particle migration depending on their particle sizes. Since the magnetophoretic repulsion force ($\vec{F}_M \sim D^3$) is more dominant than the hydrodynamic viscous drag force ($\vec{F}_D \sim D$) with respect to the particle size, large particles can migrate toward an upper channel wall at the second stage while small particles are less affected by the magnetophoretic repulsion force.

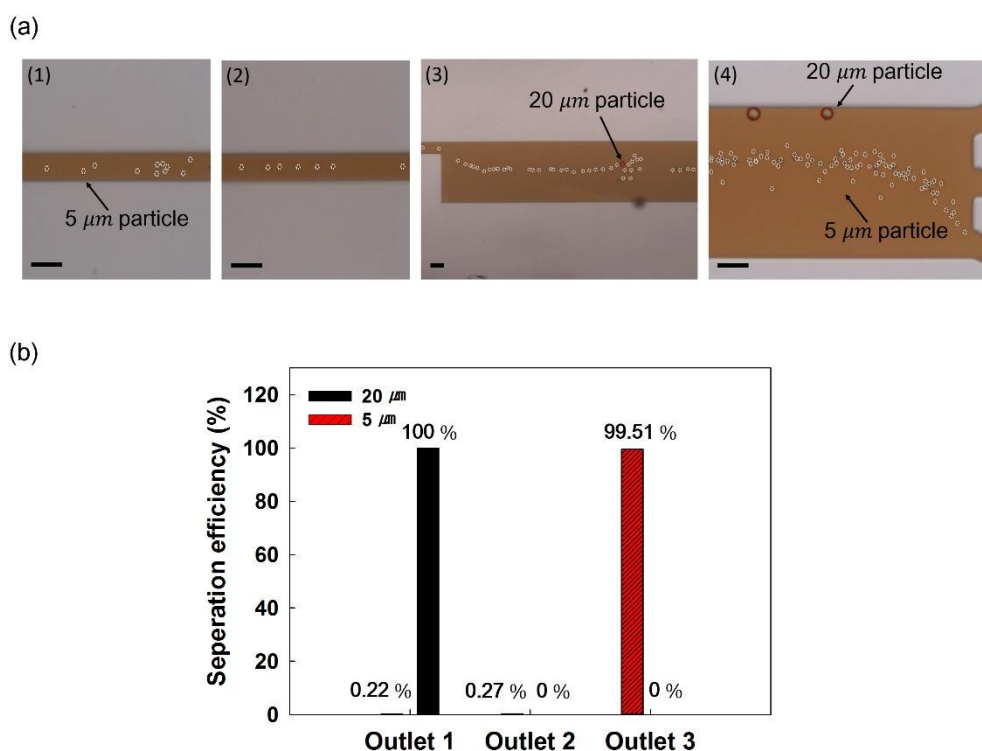


Fig. 2 Experimental results for migration of both of $20 \mu\text{m}$ and $5 \mu\text{m}$ particles. (a) Images show lateral particle migration at four different axial locations. (b) Separation efficiency of both particles at each outlet. All $20 \mu\text{m}$ particles are collected at the outlet 1 whereas most of $5 \mu\text{m}$ particles are collected at the outlet 3. A scale bar is $50 \mu\text{m}$.

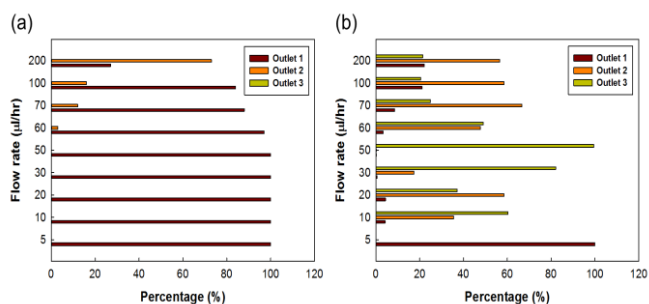


Fig. 3 Particle separation efficiency with different flow rates ranging from 5 to 200 $\mu\text{l/hr}$ for (a) 20 μm diameter and (b) 5 μm diameter particles.

The separation efficiency depends on flow rates in the microchannel since the Weissenberg number ($Wi = \lambda\dot{\gamma}_c$) and the Reynolds number ($Re = \rho U D_h / \eta_0$) are affected by flow rates. Here, λ is the relaxation time, $\dot{\gamma}_c$ is the shear rate of fluid in the channel, ρ is the density of fluid, U is the average velocity, D_h is the hydraulic diameter of channel, and η_0 is the zero-shear viscosity. The separation efficiency can also be determined by the concentration of ferrofluid since the amount of ferrofluid in the solution alters the overall magnetization of the fluid (\vec{M}_f) as well as the rheological properties of the solution (Fig. S2).

It is noted that the particles were not focused at the first stage when a Newtonian fluid was used, showing random distribution along the narrow channel (Fig. S1). For the Newtonian medium, when the magnetic field was imposed at the second stage, size dependent particle separation did not occur since the particles were not positioned along the centerline at the first stage. In this case, both of 20 μm and 5 μm particles were randomly distributed at the second stage, and 5 μm particles were prone to migrate toward the outlet 1 along with 20 μm particles, which was undesirable for the efficient particle separation. This implies that one-step particle manipulation without particle focusing prior to magnetophoretic particle migration cannot lead to successful particle separation in a microfluidic device.

As the fluid elasticity exists in the solution (meaning, the Weissenberg number, $Wi \neq 0$), a single-line particle focusing is observed in the first stage of the microchannel (Fig. 2a). It is shown that the particle focusing was successfully achieved as the particles went through the narrow microchannel from the inlet. Both 5 μm and 20 μm particles were focused along the centerline in the first stage when the flow rate was in the range of 5 to 200 $\mu\text{l/hr}$. The particle focusing was disturbed as the flow rate exceeded 200 $\mu\text{l/hr}$ due to the high inertial effect. It has been reported by Lim et al.³⁴ that the particle focusing could be achieved when $Wi \gg 0$ and $Re \gg 0$. The blockage ratio (D_p/D_h) is also an important factor for the preferential particle focusing since lift forces are dependent on the ratio of particle diameter to channel ratio, and dominate in the case of $D_p/D_h \geq 0.07$, causing particles to move toward equilibrium positions.⁶

^{8, 38} It is clearly seen that the separation efficiency for both of 5 μm and 20 μm particles was high, and all 20 μm particles were collected at the outlet 1 while 5 μm particles showed 0.22%, 0.27%, and 99.51% separation efficiencies at the outlet 1, 2, and 3, respectively (Fig. 2b). It was also found that the particle separation efficiency showed a maximum value as the flow rate was 50 $\mu\text{l/hr}$ (Fig. 3). Both 5 μm and 20 μm particles were collected at the outlet 1 when the flow rate was 5 $\mu\text{l/hr}$ due to the fact that the magnetophoretic repulsion force was much greater than the inertial force. On the other hand, the inertial force becomes greater than the magnetophoretic repulsion force as the flow rate becomes high, which deteriorates the particle separation efficiency at high flow rates. Therefore, it is advantageous to use the two step label free technique by the combination of the elastic and magnetic forces if high separation efficiency is required. For the small blockage ratio, e.g. $D_p/D_h = 0.02$, particle focusing in the viscoelastic medium was not achievable (Fig. S4). The effect of the magnetophoretic repulsion force was also not significant due to their small particle sizes.

The trajectories of two different size particles were calculated analytically to estimate the particle migration by applying the equation of motion which was given by the balance among the acceleration, hydrodynamic viscous drag and magnetophoretic repulsion forces (Fig. 4). We obtained the trajectories of the particles for the suspension with the concentration of 0.4 wt% PEO and 10 wt% ferrofluid. Both 5 μm and 20 μm particles were initially located at the same streamline before they encountered the expanded channel. 5 μm particles showed little lateral migration as they traveled downstream since they were hardly affected by the magnetic force due to the small particle sizes. On the other hand, 20 μm particles showed a linear lateral migration. The analytical results

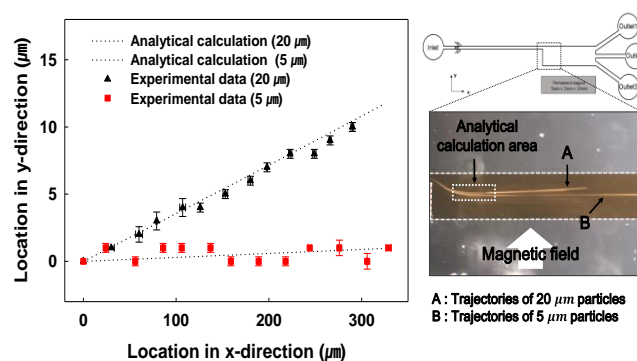


Fig. 4 Analytical calculation of the trajectories of 20 and 5 μm particles with the concentration of 0.4 wt% PEO and 10 wt% ferrofluid medium. \vec{F}_M and \vec{F}_D are two major forces to determine the position of the particles. Particles show different trajectories depending on their sizes. Experimental data are in good agreement with the analytical solution.

were in good agreement with the experimental observations. At the second stage of the microchannel, the elastic force, \vec{F}_E , can be negligible in comparison with the elastic force at the first stage in which \vec{F}_E played a major role for the particle focusing since the elasticity number (El) at the second stage were 8 times smaller than that at the first stage (Fig. S3). In this sense, \vec{F}_M and \vec{F}_D were dominant factors to determine the position of the particles at the second stage.

Since the elastic and magnetophoretic repulsion forces are associated with the concentrations of PEO and ferrofluid in the solution, the particle separation efficiency can be determined by the concentrations (Fig. 5). At lower PEO and ferrofluid concentration (PEO < 0.15 wt% and ferrofluid < 10 wt%), particles did not migrate to the center, showing random distribution at the first stage of the microchannel (Fig. 5a). When the concentration of PEO is in the range of 0.15 to 0.3 wt%, the particles tend to migrate to the center and four corners of the channel (Fig. 5c). As the concentration of ferrofluid increased to 10 wt%, the particles moved toward the upper wall, representing the lateral migration criterion by the magnetophoresis. In particular, the number of particle focusing regions was reduced to one, i.e., the centerline when the concentration of PEO increased to 0.4 wt% due to enough elasticity that pushed the particles to the center (Fig. 5e). It is found that the particles became off-centered by the

magnetophoretic repulsion force that leads the particles to move toward the upper wall of the channel over the entire range of PEO concentrations (Fig. 5f). That is, the combination of the elastic and magnetophoretic repulsion forces can generate highly efficient particle separation at certain flow conditions. Through systematic experiments, we found that the particles were focused at the center during the first stage and then separated into different outlets during the second stage when the concentrations of ferrofluid and PEO exceed 10 wt% and 0.4 wt%, respectively.

A finite element simulation was carried out to understand physics underlying the viscoelastic particle focusing and magnetophoretic particle migration (Fig. 6 and Fig. 7). The first normal stress difference, N_1 , is an indicator for the elastic force, \vec{F}_E , which is defined as $\vec{F}_E = AD_p^3 \nabla N_1$.³⁴ The normalized value ($N_1/|N_1^{max}|$) increased with an increase of Wi (Fig. 6). When Wi is zero, $N_1/|N_1^{max}|$ is zero at the cross-section since the fluid is purely viscous. As Wi increased, the elasticity of the fluid also increased, causing high $N_1/|N_1^{max}|$ at the cross-section. In particular, the minimum values were shown at four corners and the center as Wi increased, which drove the particles to move towards the center and four corners. Yang et al.³⁵ demonstrated that a single-line particle focusing at the center occurs when the fluid inertia ($Re > 0$) and the elasticity ($Wi > 0$) compete each other. We also observed the single-line particle focusing as $Re > 0.0321$ and $Wi > 1.59$.

Once the particles are focused at the center during the first stage, they flow along the streamline unless there are external forces. The fluid elasticity becomes much smaller as the

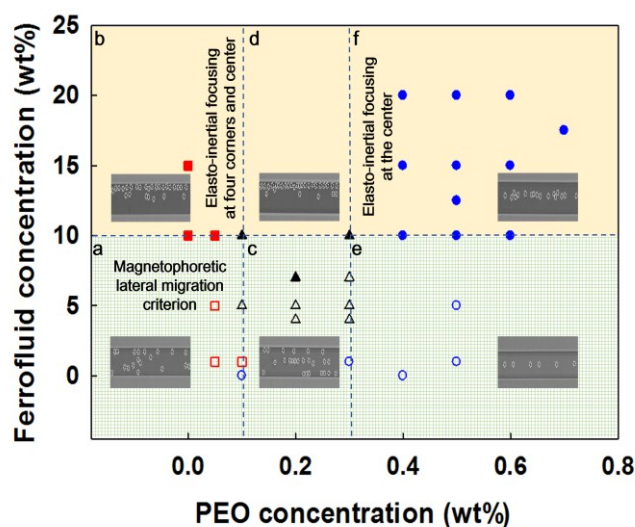


Fig. 5 Experimental results for particle dynamics as a function of PEO and ferrofluid concentrations at the first stage of a microchannel. (a) Particles show random distribution and no focusing. (b) Particles migrate toward the upper wall due to the magnetic force. (c) Particles are focused at the center and four corners. (d) Particles migrate toward the upper wall since the magnetic force surpasses the elasto-inertial force. (e) Particles are focused at the center. (f) Particles are slightly off-centered due to the combination of the elasto-inertial and magnetic forces.

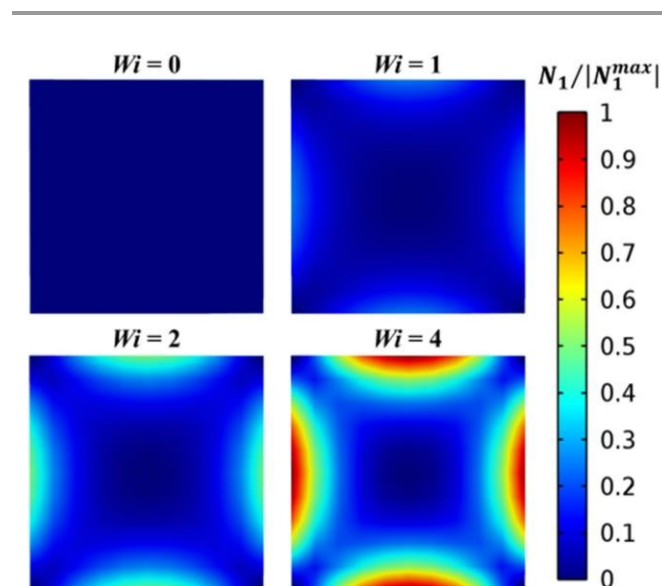


Fig. 6 Numerical simulation of the first normal stress difference (N_1). Results of the first normal stress difference with $Wi=0, 1, 2,$ and 4 in the straight square channel. $N_1/|N_1^{max}|$ shows symmetry at the cross-section of the microchannel, and increases with increasing Wi .

Surface: Magnetic flux density norm (T), Arrow: Magnetic flux density

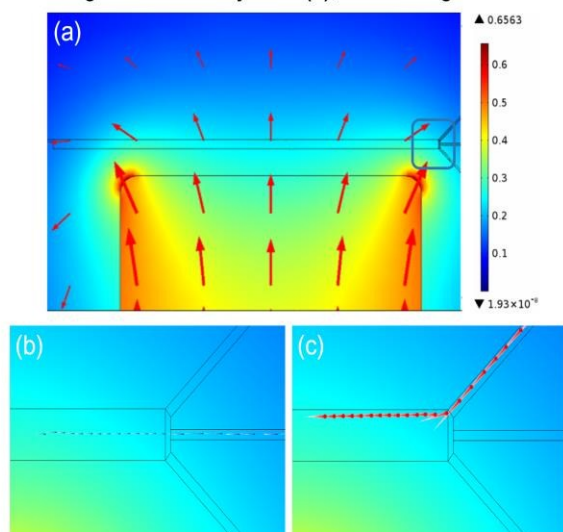


Fig. 7 Numerical simulation of magnetophoretic particle separation. (a) A whole microfluidic system showing the magnetic field and microfluidic channel. (b) 5 μm particles are collected at the outlet 2, (c) whereas 20 μm particles are collected at the outlet 1 due to the effect of magnetophoretic repulsion (\vec{F}_M) and hydrodynamic viscous drag forces (\vec{F}_D). Large particles migrate toward the upper wall of the microchannel since the magnetophoretic repulsion force is proportional to a_r^3 whereas the hydrodynamic viscous drag force is proportional to a_r^2 .

particles pass through the second stage with a high channel aspect ratio since the elasticity number becomes almost a tenth of the values at the first stage (Fig. S3). Therefore, the effect of the elasticity can be neglected in the expanded channel. On the other hand, the magnetophoretic repulsion force is determined by the magnetization of the solution and the external magnetic force. While the particles pass through the expanded channel, they undergo lateral migration due to the magnetophoretic repulsion force, \vec{F}_M , and the hydrodynamic viscous drag force, \vec{F}_D . We performed numerical simulations to investigate the effect of the magnetic force and the magnetization on the particle migration and separation (Fig. 7). The strength of the magnetic field is proportional to the magnetic force generated by the magnet at the bottom of the channel, and an asymmetric magnetic field is generated to cause the lateral migration of the particles (Fig. 7a). It is clearly seen that different sized particles could be collected at different outlets. Since 5 μm particles were less influenced by the magnetophoretic repulsion force in comparison with 20 μm particles, they were collected at the outlet 2 (Fig. 7b). However, 20 μm particles were prone to move toward the upper wall of the channel and collected at the outlet 1 (Fig. 7c). The simulation results demonstrate that the combination of \vec{F}_E and \vec{F}_M is essential for an efficient label free particle separation through a two-step microfluidic platform by

utilizing the elasto-inertial focusing and negative magnetophoresis.

Further experiments were carried out with two different sized biological cells (*Chlorella vulgaris* and *Synechococcus sp.*) since the isolation and separation of rare cells are of importance for a variety of biological applications. The average diameters of *Chlorella vulgaris* and *Synechococcus sp.* are found to be 5.26 μm and 2.51 μm , respectively (Fig. S5a and S5b). It is shown that *Chlorella vulgaris* cells are focused at the center of the microchannel by the elastic force and migrate toward an upper wall due to the external magnetic force (Fig. S5c and S5e). Therefore, *Chlorella vulgaris* cells are collected at an outlet 1. On the other hand, *Synechococcus sp.* cells are affected by neither the elastic force nor the magnetic force, showing random distribution as flowing downstream in the channel since the sizes of the cells are relatively smaller than the channel width, and the blockage ratio is only 0.05, which is insufficient to generate the viscoelastic particle focusing (Fig. S5d and S5f). Our ongoing effort is to optimize cell separating conditions by considering the deformation of cells and their viscoelasticity.

Conclusions

We developed a facile two step label free particle separation technique via elastic and magnetophoretic repulsion forces. The particles were focused at the center of the narrow channel due to the elastic force at the first stage followed by a differential migration depending on their sizes by the magnetophoretic repulsion force at the second stage. This strategy is simple, but a robust way to achieve highly efficient particle separation. The trajectories of the two different sized particles were calculated analytically to demonstrate the particle migration by applying the equation of motion that is derived by a force balance among the acceleration, hydrodynamic viscous drag, and magnetophoretic repulsion forces. We also performed numerical simulations to investigate the effect of fluid elasticity and particle migration due to the magnetophoretic repulsion force. These numerical calculations provided comprehensive understanding on the mechanism of the particle focusing and lateral migration. We envision that these theoretical and experimental studies provide in-depth insight for developing label free particle and cell separation in microfluidic systems.

Methods

Fabrication and design of devices: The microfluidic devices were fabricated by using a standard soft lithography technique. The base and curing agents of PDMS with 10:1 mixing ratio (Sylgard 184, Dow Corning) was poured onto the SU-8 photoresist mold, degassed in a vacuum chamber, and cured in an oven at 70°C for 6 hr. The devices were cut from the mold, and punched with a sharpened flat-tip needle to make inlets and outlets. The PDMS replica was bonded onto the slide glass after oxygen plasma treatment. Then, the devices were placed on a hotplate at 120 °C for 20 min to increase bonding strength. A NdFeB permanent magnet was positioned by the side of the microchannel as shown in Fig. 1. The magnetic flux density of the

magnet was measured to be 0.198 Tesla by using a Tesla meter (TM-701, KANETEC).

Sample preparation: Three types of polystyrene (PS) particles were used in these experiments. 1 μm PS particles (R0100, Thermo scientific), 5 μm PS particles (PS06N, Bangs Laboratories) and 20 μm PS particles (18329-5, Polysciences) were dispensed into Newtonian and viscoelastic fluids. The Newtonian fluid was prepared with 22 wt% aqueous glycerol solution to match the densities between the fluid and PS particles (1.05 g/ml).²⁰ For the viscoelastic fluid, Poly(ethylene oxide) (PEO) ($M_w = 1,000,000$, Sigma Aldrich) was diluted in 22 wt% aqueous glycerol solution. A water based ferrofluid (EMG 408, Ferrotec Corp.) was mixed with the fluids. A small amount of surfactant (Tween 20, Sigma-Aldrich) was added to both of solutions to prevent particle aggregation. Two different sized biological cells (*Chlorella vulgaris* and *Synechococcus sp.*) were cultured with BG11 medium (C3061, Sigma Aldrich) for 14 days before usage. Particles and cells were extracted from the medium after experiments by a magnet (Fig. S6). To investigate the viability of cells, 1% Evans blue dye (EBD) in phosphate-buffered saline (PBS, pH 7.5) was used. For testing the viability of *Chlorella vulgaris* cells with EBD, *Chlorella vulgaris* cells were incubated in the dye prior to introducing the cell solution into a microchannel. Then, the cell solution was collected from the outlet after an experiment to investigate the viability. Dead cells are distinguished by a dark-blue color, whereas viable cells are not stained by EBD, which gives different light intensity peaks (Fig. S7a and S7b). It is shown that the viability of the cells decays slowly with respect to time, but more than 60 % *Chlorella vulgaris* cells are still viable after a day in the PEO/ferrofluid solution (Fig. S7c).

Measurement of rheological properties: The relaxation time of viscoelastic fluids was measured using a capillary break-up extensional rheometer (CaBER, ThermoHaake).³⁹ It was found that the midpoint filament radius, $R_{mid}(t)$, decreased exponentially with time and showed such relationship with the characteristic relaxation time (λ_c) of the solution as $R_{mid}(t) = R_1 \exp(-t/\lambda_c)$, where R_1 is the initial radius of the filament.³⁸ The viscosity of each fluid was measured by using a strain controlled rheometer (AR G2, TA Instruments) with 60 mm diameter parallel plates over the shear rate of $1 \leq \dot{\gamma} \leq 1000 \text{ s}^{-1}$ (Fig. S2). The measured data were fitted with the Carreau model to estimate the zero shear rate and infinite shear rate viscosities, which is expressed by $(\eta - \eta_\infty)/(\eta_0 - \eta_\infty) = 1/(1 + (\lambda\dot{\gamma})^2)^{n/2}$ where n is the power index, λ is the relaxation time, and the values are listed in Table S2.

Analytical calculation: The trajectories of different size particles for the solution with the concentration of 0.4 wt% PEO and 10 wt% ferrofluid were calculated analytically as below.

$$L_x = L_{ix} + \int_0^t v_{p,x}(t) dt, \quad L_y = L_{iy} + \int_0^t v_{p,y}(t) dt \quad (1)$$

where L_x and L_y are the instantaneous x-location and y-location of the particle, L_{ix} and L_{iy} are the initial x-location and initial y-location of the particle, $v_{p,x}$ and $v_{p,y}$ are the particle velocities in the x-direction and y-direction, and t is the reference time (Fig. 4). We

neglected the contribution of the magnetophoretic repulsion force to the horizontal direction since the magnet is positioned at the bottom of the channel wall.⁴⁰ The analytical expression for the magnitude of magnetic field caused by the rectangular magnet with the thickness T , width W , and length L is expressed as,

$$H(y) = \frac{M_s}{\pi} \left[\tan^{-1} \left(\frac{y + T\sqrt{W^2 + L^2 + (y+T)^2}}{WL} \right) - \tan^{-1} \left(\frac{y\sqrt{W^2 + L^2 + y^2}}{WL} \right) \right] \quad (2)$$

All the parameters involved in the modeling are listed in Table S1. It is assumed that the fluid velocity along the x-direction ($v_{f,x}$) is equal to the particle velocity ($v_{p,x}$). The entrance length correlates with the Reynolds number for a laminar flow, which can be expressed as $L_e \approx 0.06Re$. Therefore, a fully developed laminar flow is assumed in this condition. Thus, the velocity profile for the fully developed laminar flow is given by

$$v_{f,x} = v_{p,x} = 3Q/(8w_c h_c) \left[1 - \left(\frac{y}{w_c} \right)^2 \right] \quad (3)$$

In which Q is volumetric flow rate, w_c is the width, and h_c is the height of the microchannel, respectively. The equation of motion of particles under the Stokes flow is $m_p d\vec{v}_p/dt = \vec{F}_M + \vec{F}_D$. This equation is modified as $m_p dv_{p,y}/dt = F_{M,y} + F_{D,y}$ by considering the magnetophoretic repulsion force acting on the particle along the y-direction. Here, $F_{M,y}$ is defined as $F_{M,y} = -2\pi\mu_0\phi a_p^3 M_d L(\alpha) \nabla H^2 / 3H$, in which ϕ is the volume fraction of magnetic nanoparticles, M_d is the saturation magnetization of the ferrofluid, $L(\alpha)$ is the Langevin function, and H is the magnitude of the magnetic field, μ_0 is the permeability of free space, and a_p is radius of the spherical diamagnetic particle. By assuming the fluid flow is laminar in the x-direction, $v_{f,y}$ is neglected. Thus, $F_{D,y}$ is reduced to $F_{D,y} = -3\pi\eta D_p v_{p,y} / f_D$. The magnetophoretic repulsion force is proportional to the volume of the particle, and the hydrodynamic viscous drag force is proportional to the diameter of the particle. We obtain the particle velocity in the y-direction ($v_{p,y}$) as below.

$$v_{p,y} = -\mu_0\phi a_p^2 M_d L(\alpha) \nabla H^2 / (9\eta f_D H) \left(1 - e^{-\frac{6\pi a_p \eta f_D t}{m_p}} \right) \quad (4)$$

The trajectories of the particles with different sizes can be determined by substituting equations (3) and (4) into equation (1).

Numerical simulation: The Oldroyd-B model is used to estimate the fluid elasticity depending on the Weissenberg number in the first stage of the microchannel. The first normal stress difference is calculated while varying the Weissenberg number, $Wi = \lambda\dot{\gamma}_c$, which helps understand the particle focusing behavior with enhanced fluid elasticity at the first stage of the microchannel. For the simulation, governing equations are non-dimensionalized by using Re and Wi . For a steady state, the momentum equation is expressed as $Re(\mathbf{u} \cdot \nabla)\mathbf{u} = \nabla \cdot (-p\mathbf{I} + (\eta_s/\eta)[(\nabla\mathbf{u}) + (\nabla\mathbf{u})^T] + \mathbf{T})$ and the extra stress contribution becomes $\mathbf{T} + Wi\mathbf{T} = (\eta_p/\eta)[(\nabla\mathbf{u}) + (\nabla\mathbf{u})^T]$,

where $\overset{\nabla}{T}$ is the upper convected derivative operator expressed as $\overset{\nabla}{T} = \partial T / \partial t + (u \cdot \nabla)T - [(\nabla u) \cdot T + T \cdot (\nabla u)^T]$, λ is the characteristic relaxation time, η_p is the relative polymer viscosity, η_s is the relative solvent viscosity, and the total viscosity is $\eta = \eta_s + \eta_p$. The relative solvent and polymer viscosities are set to 0.6 and 0.4, respectively. Wi is varied to observe the effect of N_1 . Once particles are aligned along the centerline due to the fluid elasticity, they flow along their streamlines to downstream. The Carreau model as a Non-Newtonian viscosity model is used to model the particle migration in a fluid in the entire microchannel, whose parameters are set to $\lambda = 0.00634$, $\eta_0 = 9.08 \times 10^{-3} \text{ Pa} \cdot \text{s}$, $\eta_\infty = 7.21 \times 10^{-7} \text{ Pa} \cdot \text{s}$, and $n = 0.1056$ according to the rheological properties of the fluids (Fig. S2). In this magnetostatic problem, where no electric current is present, $\nabla \times H = 0$, which implies the magnetic scalar potential is given by $H = -\nabla\psi$. By adding the constitutive relation of $B = \mu_0(H + M)$ into $\nabla \cdot B = 0$, the equation becomes $\nabla \cdot (\mu_0 \nabla\psi - \mu_0 M) = 0$, where μ_0 is the permeability of a vacuum and M is the magnetization of a permanent magnet. The lifting force (F_L) acting on the particle is determined by $d(m_p V) / dt = F_L$, which is the combination of the hydrodynamic viscous drag force (F_D) and the magnetophoretic repulsion force (F_M). The two forces are expressed as $F_D = 18m_p \eta (U - V_p) / 4\rho_p a_p^2$ and $F_M = 2\pi a_p^3 \mu_0 \mu_{r,f} K \nabla H^2$, where m_p is the density of particle, η is the fluid dynamic viscosity, U is the fluid velocity, V_p is the particle velocity, ρ_p is the particle density, a_p is the particle radius, $\mu_{r,f}$ is the fluid relative permeability, $\mu_{r,p}$ is the particle relative permeability, and K is defined as $(\mu_{r,p} - \mu_{r,f}) / (\mu_{r,p} + 2\mu_{r,f})$. Overall, the momentum equation, magnetic field, and particle tracing are consecutively solved to obtain the lateral migration of the particles depending on their sizes.

Acknowledgements

This research was supported by the Korea Science and Engineering Foundation (KOSEF) grant funded by the Korean government (MEST) (R11-2005-065) through the Intelligent Textile System Research Center (ITRC). It was partially supported by Basic Research Program through the National Research Foundation of Korea (NRF) funded by the Ministry of Education, Science and Technology (2015R1A6A3A03020612 and 2013R1A1A2059827). It was also supported by the Commercializations Promotion Agency for R&D Outcomes (COMPA) funded by the Ministry of Science, ICT and Future Planning (MISP), and the Industrial Strategic Technology Development Program funded by the Ministry of Trade, Industry & Energy (MI, Korea) (10052641). The authors are grateful for the support.

Notes and references

1. J. P. Nolan and L. A. Sklar, *Nat Biotechnol*, 1998, **16**, 633-638.
2. X. H. Cheng, D. Irimia, M. Dixon, K. Sekine, U. Demirci, L. Zamir, R. G. Tompkins, W. Rodriguez and M. Toner, *Lab Chip*, 2007, **7**, 170-178.
3. M. Antia, T. Herricks and P. K. Rathod, *Cell Microbiol*, 2008, **10**, 1968-1974.
4. P. Gascoyne, J. Satayavivad and M. Ruchirawat, *Acta Trop*, 2004, **89**, 357-369.
5. A. van de Stolpe, K. Pantel, S. Sleijfer, L. W. Terstappen and J. M. J. den Toonder, *Cancer Res*, 2011, **71**, 5955-5960.
6. J. Nam, H. Lim, D. Kim, H. Jung and S. Shin, *Lab Chip*, 2012, **12**, 1347-1354.
7. M. M. Wang, E. Tu, D. E. Raymond, J. M. Yang, H. Zhang, N. Hagen, B. Dees, E. M. Mercer, A. H. Forster and I. Kariv, *Nat Biotechnol*, 2005, **23**, 83-87.
8. S. Miltenyi, W. Muller, W. Weichel and A. Radbruch, *Cytometry*, 1990, **11**, 231-238.
9. T. T. Zhu, F. Marrero and L. D. Mao, *Microfluid Nanofluid*, 2010, **9**, 1003-1009.
10. A. Karimi, S. Yazdi and A. M. Ardekani, *Biomicrofluidics*, 2013, **7**.
11. A. A. S. Bhagat, S. S. Kuntaegowdanahalli and I. Papautsky, *Microfluid Nanofluid*, 2009, **7**, 217-226.
12. D. Di Carlo, D. Irimia, R. G. Tompkins and M. Toner, *P Natl Acad Sci USA*, 2007, **104**, 18892-18897.
13. S. A. Soper, K. Brown, A. Ellington, B. Frazier, G. Garcia-Manero, V. Gau, S. I. Gutman, D. F. Hayes, B. Korte, J. L. Landers, D. Larson, F. Ligler, A. Majumdar, M. Mascini, D. Nolte, Z. Rosenzweig, J. Wang and D. Wilson, *Biosens Bioelectron*, 2006, **21**, 1932-1942.
14. A. J. Tudos, G. A. J. Besselink and R. B. M. Schasfoort, *Lab Chip*, 2001, **1**, 83-95.
15. H. W. Hou, A. A. S. Bhagat, A. G. L. Chong, P. Mao, K. S. W. Tan, J. Y. Han and C. T. Lim, *Lab Chip*, 2010, **10**, 2605-2613.
16. A. Higuchi and Y. Tsukamoto, *J Biomed Mater Res A*, 2004, **71A**, 470-479.
17. Y. Ito and K. Shinomiya, *J Clin Apheresis*, 2001, **16**, 186-191.
18. K. W. Kwon, S. S. Choi, S. H. Lee, B. Kim, S. N. Lee, M. C. Park, P. Kim, S. Y. Hwang and K. Y. Suh, *Lab Chip*, 2007, **7**, 1461-1468.
19. T. Laurell, F. Petersson and A. Nilsson, *Chem Soc Rev*, 2007, **36**, 492-506.
20. L. T. Liang, S. Qian and X. C. Xuan, *J Colloid Interf Sci*, 2010, **350**, 377-379.
21. N. Pamme and A. Manz, *Anal Chem*, 2004, **76**, 7250-7256.
22. R. Pethig, *Biomicrofluidics*, 2010, **4**.
23. R. E. Rosensweig, *Ferrohydrodynamics*, Courier Dover Publications, 1997.
24. W. M. Deen, *Analysis of transport phenomena*, Oxford University Press, New York, 1998.
25. J. P. Liu, *Nanoscale magnetic materials and applications*, Springer Verlag, New York, NY, 2009.
26. A. Sinha, R. Ganguly, A. K. De and I. K. Puri, *Phys Fluids*, 2007, **19**.
27. T. T. Zhu, D. J. Lichlyter, M. A. Haidekker and L. D. Mao, *Microfluid Nanofluid*, 2011, **10**, 1233-1245.
28. L. T. Liang and X. C. Xuan, *Microfluid Nanofluid*, 2012, **13**, 637-643.
29. A. Winkleman, K. L. Gudiksen, D. Ryan, G. M. Whitesides, D. Greenfield and M. Prentiss, *Appl Phys Lett*, 2004, **85**, 2411-2413.
30. J. Zeng, C. Chen, P. Vedantam, V. Brown, T. R. J. Tzeng and X. C. Xuan, *J Micromech Microeng*, 2012, **22**.
31. T. T. Zhu, R. Cheng, Y. F. Liu, J. He and L. D. Mao, *Microfluid Nanofluid*, 2014, **17**, 973-982.
32. S. Caserta, G. D'Avino, F. Greco, S. Guido and P. L. Maffettone, *Soft Matter*, 2011, **7**, 1100-1106.
33. K. Kang, S. S. Lee, K. Hyun, S. J. Lee and J. M. Kim, *Nat Commun*, 2013, **4**.

Journal Name

ARTICLE

34. E. J. Lim, T. J. Ober, J. F. Edd, S. P. Desai, D. Neal, K. W. Bong, P. S. Doyle, G. H. McKinley and M. Toner, *Nat Commun*, 2014, **5**.
35. S. Yang, J. Y. Kim, S. J. Lee, S. S. Lee and J. M. Kim, *Lab Chip*, 2011, **11**, 266-273.
36. S. Yang, S. S. Lee, S. W. Ahn, K. Kang, W. Shim, G. Lee, K. Hyun and J. M. Kim, *Soft Matter*, 2012, **8**, 5011-5019.
37. D. J. Lee, H. Brenner, J. R. Youn and Y. S. Song, *Sci Rep-Uk*, 2013, **3**.
38. G. H. McKinley and A. Tripathi, *J Rheol*, 2000, **44**, 653-670.
39. L. E. Rodd, T. P. Scott, J. J. Cooper-White and G. H. McKinley, *Appl Rheol*, 2005, **15**, 12-27.
40. E. P. Furlani, *Permanent magnet and electromechanical devices : materials, analysis, and applications*, Academic, San Diego, Calif., 2001.

TOC figure

High separation efficiency of particles and cells can be realized by exploiting a facile two step label free technique that consists of the elasto-inertial focusing and magnetophoresis.

